High temperature stability, metallic character and bonding of the Si_2BN planar structure

IOP Publishing Journal of Physics: Condensed Matter
J. Phys.: Condens. Matter **33** (2021) 165001 (15pp) https://doi.org/10.1088/1361-648X/abdbe9

High temperature stability, metallic character and bonding of the Si_2BN planar structure

Zacharias G Fthenakis[1,2,3,*], Meghnath Jaishi[4], Badri Narayanan[4], Antonis N Andriotis[5] and Madhu Menon[6,7]

[1] Theoretical and Physical Chemistry Institute, National Hellenic Research Foundation, GR-11635, Athens, Greece
[2] Department of Surveying and Geoinformatics Engineering, University of West Attica, GR-12243, Athens, Greece
[3] Department of Marine Engineering, University of West Attica, GR-12243, Athens, Greece
[4] Department of Mechanical Engineering, University of Louisville, Louisville, Kentucky 40292, United States of America
[5] Institute of Electronic Structure and Laser, FORTH, PO Box 1527, 71110 Heraklio, Crete, Greece
[6] Conn Center for Renewable Energy Research, University of Louisville, Louisville, KY 40292, United States of America
[7] Department of Physics and Astronomy, University of Kentucky, Lexington, KY 40506, United States of America

E-mail: fthenak@eie.gr, zfthenakis@uniwa.gr and super250@g.uky.edu

Received 31 August 2020, revised 15 December 2020
Accepted for publication 14 January 2021
Published 10 March 2021

Abstract

The family of monolayered Si_2BN structures constitute a new class of 2D materials exhibiting metallic character with remarkable stability. Topologically, these structures are very similar to graphene, forming a slightly distorted honeycomb lattice generated by a union of two basic motifs with AA and AB stacking. In the present work we study in detail the structural and electronic properties of these structures in order to understand the factors which are responsible for their structural differences as well as those which are responsible for their metallic behavior and bonding. Their high temperature stability is demonstrated by the calculations of finite temperature phonon modes which show no negative contributions up to and beyond 1000 K. Presence of the negative thermal expansion coefficient, a common feature of one-atom thick 2D structures, is also seen. Comparison of the two motifs reveal the main structural differences to be the differences in their bond angles, which are affected by the third nearest neighbor interactions of *cis–trans* type. On the other hand, the electronic properties of these two structures are very similar, including the charge transfers occurring between orbitals and between atoms. Their metallicity is mainly due to the p_z orbitals of Si with a minor contribution from the p_z orbitals of B, while the contribution from the p_z orbitals of N atoms is negligible. There is almost no contributions from the N p_z electrons to the energy states near the Fermi level, and they form a band well below it. I.e., the p_z electrons of N are localized mostly at the N atoms and therefore cannot be considered as mobile electrons of the p_z cloud. Moreover, we show that due to the relative positions in the energy axis of the atomic energies of the p_z orbitals of B, N and Si atoms, the density of states (DOS) of Si_2BN can be considered qualitatively as a combination of the DOS of planar hexagonal BN (h-BN) and hypothetically planar silicene (ph-Si). As a result, the Si_2BN behaves electronically at the Fermi level as

*Author to whom any correspondence should be addressed.

slightly perturbed ph-Si, having very similar electronic properties as silicene, but with the advantage of having kinetic stability in planar form. As for the bonding, the Si–Si bonds are covalent, while the π back donation mechanism occurs for the B–N bonding, in accordance with the B–N bonding in h-BN.

Keywords: 2D material, electronic structure, first principles calculations, molecular dynamics, nano electronics

(Some figures may appear in colour only in the online journal)

1. Introduction

The last one and a half decade has seen a huge amount of effort invested in the prediction, design and synthesis of novel two-dimensional (2D) materials as well as in the study of their properties. This increasing interest in 2D materials is driven by their unique properties [1], which are expected to bring technology to new Frontiers in the near future. Beginning with the isolation of graphene [2, 3]—the most celebrated 2D material—the list of 2D materials, which have either been synthesized or theoretically predicted, has been significantly expanded. These include several graphene allotropes [4–8], hexagonal BN [9, 10], several transition metal dichalcogenide monolayers [11], such as MoS_2 [12], phosphorene [13], silicene [14–16], germanene [16], as well as several others (see, for instance, references [9, 17–22]).

Silicon based 2D materials [9, 14–16, 18–22] have also been studied. However, most of them with three fold coordinated Si atoms have low stability, due to the preference of Si to form sp^3 instead of sp^2 bonds. On general grounds, it is energetically more favorable for Si atoms in a three-fold coordinated geometry to form dangling bonds rather than the delocalized cloud of π bonds between adjacent p_z orbitals. As a result this has the effect of turning the structure into a chemically reactive one rather than a stable planar one. Avoidance of dangling bonds is therefore a crucial requirement for kinetic (or even thermodynamic) stability in a planar form.

To the best of our knowledge, very few Si-based planar structures have been investigated and found to be planar, like, for instance, the honeycomb SiC and Si_3X [18–20] structures, with X = B, C and Al. Very recently, the authors have proposed a stable graphene-like single layered Si_2BN structure that is free of dangling bonds and entirely flat with unusual sp^2 like bonding for all Si atoms [23]. In this structure each Si atom has a Si, B, and N nearest neighbor, while each B (N) has two Si's and one N (B) as nearest neighbors and possesses *Cmmm* symmetry (figure 1(a), top). The stability of the Si_2BN structure has been verified using frequency analysis as well as high temperature molecular dynamics simulations. Topologically it can be considered as a honeycomb structure composed of a parallel arrangement of Si–Si dimers along the x direction, which are directed along the y direction and connected with alternating B–N and N–B dimers, also directed along the y direction, which are also parallely arranged with each other along the x direction.

Soon after the publication of that study, another study [24] proposed a second Si_2BN structure with *Pmma* symmetry which differs from the original one in a slight rearrangement of the B and N atoms (figure 1(b), top). This structure was found to be marginally more stable than the first one.

The unique composition and properties of Si_2BN show potential applications beyond graphene and has generated much interest in the scientific community. It has been characterized with respect to its mechanical [25] and electronic [26] properties. It has been proposed as host material for hydrogen storage [27, 28] and as anode for Li and Na ion batteries [29]. It has been found to be an efficient sensor for gases such as N [30] as well as CO, NH_3 and NO molecules [31]. Studies have also been performed for its HCN absorption capacity [32] and thermoelectric efficiency [33]. It has been shown to be a promising candidate for euryphotic photosensitive detector applications [34]. Si_2BN flakes and derivatives have been investigated as a potential material for Li^+ ion and CO_2 adsorption [35, 36]. The optoelectronic properties of Si_2BN quantum dots have also been studied [37]. Singh *et al* have reported enhancement of hydrogen evolution reaction activity on a Si_2BN monolayer [38]. Electronic and optical properties of Si_2BN/MoS_2 heterostructures have been investigated [39]. Moreover, its structure has inspired the design and study of other similar materials like the family of Pb_2XY 2D topological insulators, with X = Ga/In and Y = Sb/Bi [40], the family of $Ge_x(BN)_y$ structures [41] and the IV–V–VI compounds [42].

In this work we present our detailed analysis of the bonding in the Si_2BN structures that reveals a delicate interplay between the structural and electronic properties and explain the origin of metallicity in this system. We begin by a close examination of the two Si_2BN isomers shown in figure 1 (top). As seen in the figure, their structural difference results from the different ways of stacking the B–N dimers. I.e., the structure in figure 1(b) (top) can be obtained by moving the alternate rows of B–N dimers in figure 1(a) (top) along the x-direction. This is illustrated schematically with arrows in figure 1 (bottom) where we assign stacking labels AA and AB for structures in figure 1(b) (top) and figure 1(a) (top), respectively. I.e., in the left panel of figure 1 (bottom), the B–N dimers have AA stack-

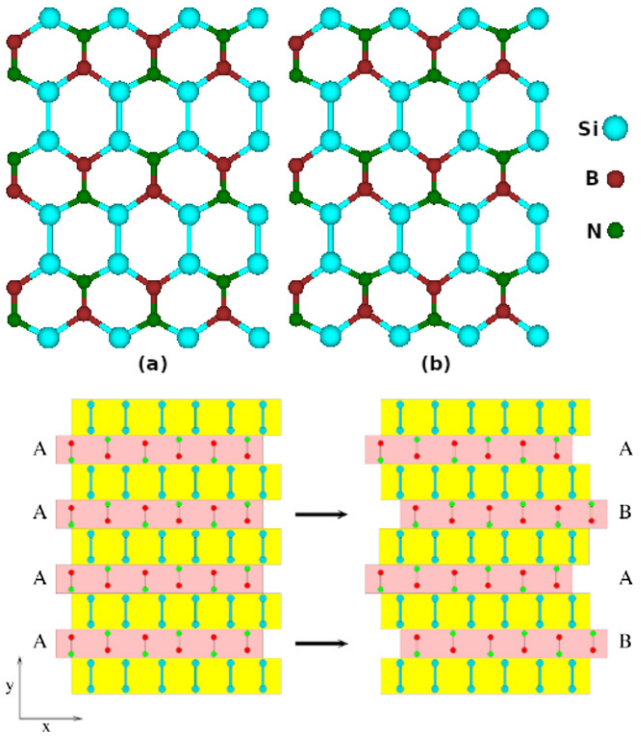

Figure 1. The two optimized planar Si_2BN structures (top). Figure showing schematically the AA and AB stacking of Si_2BN structure (bottom left and bottom right panel, respectively). Si–Si and B–N bond arrays are shown with yellow and pink ribbons, respectively, alternating with each other along *y* direction. The arrows at the center of the figure show the shifted pink ribbons of B–N bonds, which turn the structure from the left one (with AA stacking) to the right one (with AB stacking).

ing along the *y* direction, while in the structure shown in the right panel, they have AB stacking. In the schematic representation shown in figure 1 (bottom), the parallel arrangement of Si–Si bonds is shown as yellow ribbons, while the parallel arrangement of the alternating B–N and N–B bonds as pink ribbons. Those ribbons (yellow and pink) alternate with each other along the *y* direction, thus forming the proposed Si_2BN structure. The two different stackings described above can be used as a basis for generating a whole family of Si_2BN structures, which can be built with different combinations of such 'A' and 'B' ribbons. Due to the exceptional stability of the Si_2BN structures with AA and AB stacking, there is no reason for any member of that family to be unstable. Bearing in mind that 'A' and 'B' type of those ribbons can represent 0 and 1, it is easy to understand the potential application of those Si_2BN structures to be used as information storage devices at the atomic scale.

In the present study we perform optimization calculations for Si_2BN with AA and AB stackings and compare our results with planar silicene (ph-Si) and hexagonal BN (h-BN) structures. We show that Si_2BN with either AA or AB stacking can be seen as extensively doped silicene [16] structures, which while behaving electronically very similar to silicene (as already explained), has the added advantage of being entirely flat (without any dangling bonds) and demonstrating extreme kinetic stability. This should be contrasted with the original silicene which is buckled and exhibits kinetic instability, with unsaturated dangling bonds making it highly reactive [16]. A detailed study of the structural and electronic properties are therefore essential for shedding light on the factors that are responsible for their structural differences as well as their metallic behavior and bonding.

We find that the main distinguishing feature between the two structures are the differences in their bond angles, which are caused by the third nearest neighbor interactions of *cis–trans* type. Moreover, we find that its metallic character is mainly due to the p_z electrons of Si with a minor contribution from the p_z electrons of B. The p_z occupied states of N are mostly localized on the N atoms and are situated well below the Fermi level and therefore provide a negligible contribution at the Fermi level. Small contributions from the $3d_{zx}$ and $3d_{yz}$ orbitals of Si also occur at the Fermi level. The metallic character of Si_2BN with AA stacking comes from the band crossing at the Γ point, while for the Si_2BN with AB stacking this comes both from the band crossing near the Γ and the two *X* points (i.e. the center and two of the six corners of the almost hexagonal Brillouin zone). This should be contrasted with graphene whose semi-metallicity comes from the vertices of the Dirac cones, which appear at the six corners of its perfectly hexagonal Brillouin zone.

Furthermore, we show that, qualitatively, due to the relative positions on the energy axis of the atomic energies of the p_z orbitals of B, N and Si atoms, the DOS of Si_2BN near the Fermi level can be considered as a combination of the DOS of the planar h-BN and the hypothetically ph-Si. As a result, the two Si_2BN structures of our study behave electronically as slightly perturbed ph-Si structures, having very similar electronic properties with silicene, while also possessing the benefit of planarity and kinetic stability, as already stated. Having a behavior similar to silicene at the Fermi level, Si_2BN can be readily turned into a semiconductor, if subjected to techniques that are used to open a gap in silicene or graphene (for instance by applying an electric field [43], by superhalogen [44] or Na atom [45] absorption, etc) are applied.

2. The method

Our optimization calculations were performed using the density functional theory method in the generalized gradient approximation (GGA) level utilizing the Perdue–Burke–Ernzerhof (PBE) functional [46] as implemented in the SIESTA code [47]. The effect of core electrons is simulated by pseudopotentials. For our calculations we utilize the norm-conserving Troullier–Martins pseudopotentials [48] in the Kleinman–Bylander factorized form [49]. These pseudopotentials can be found in the SIESTA GGA pseudopotential database [50]. SIESTA uses atomic-like basis sets in real space for the construction of a Bloch wavefunction basis set in the reciprocal space, onto which the wavefunctions of the system are expanded. The atomic like basis set (in real space) used in our calculations, is the standard double-zeta basis with polarization orbitals for each atom used by SIESTA. The *k*-points grid of the reciprocal space used, varies depending on the system. The mesh cutoff energy for the

Table 1. Theoretically predicted crystallographic data for Si_2BN with AA and AB stacking.

	Si_2BN AA stacking	Si_2BN AB stacking
Space group	51 *Pmma* orthorhombic	65 *Cmmm* BC orthorhombic
a, b, c (Å)	6.3918, 5.6420, 20	6.4204, 11.2932, 20
α, β, γ (deg)	90, 90, 90	90, 90, 90
[a] a, b, c (Å)		6.4954, 6.4954, 20
"[a]α, β, γ (deg)".|		90, 90, 120.7619
Wyckoff	(0, 0, 0)+	(0, 0, 0)+
Positions		(1/2, 1/2, 0)+
Si	j (multiplicity 4)	q (multiplicity 8)
	$x = 0.499\,68$	$x = 0.244\,72$
	$y = -0.200\,33$	$y = -0.399\,86$
Positions:	$(x, y, 0)$	$(x, y, 0)$
	$(-x, -y, 0)$	$(-x, -y, 0)$
	$(x, -y, 0)$	$(x, -y, 0)$
	$(-x, y, 0)$	$(-x, y, 0)$
B	f (multiplicity 2)	h (multiplicity 4)
	$y = -0.404\,32$	$y = -0.197\,00$
Positions:	$(1/4, y, 0)$	$(0, y , 0)$
	$(3/4, -y, 0)$	$(0, -y, 0)$
N	f (multiplicity 2)	h (multiplicity 4)
	$y = 0.336\,03$	$y = -0.326\,67$
Positions:	$(1/4, y, 0)$	$(0, y, 0)$
	$(3/4, -y, 0)$	$(0, -y, 0)$
Bond lengths (Å)		
Si–Si	2.261	2.262
Si–B	1.968	1.970
Si–N	1.774	1.776
B–N	1.465	1.465
Bond angles deviations from 120° (deg)		
$\delta\phi_1$	−11.60	−7.42
$\delta\phi_2$	8.86	4.49
δ	0.11	0.00

[a]Hexagonal setting.

determination of charge densities and potentials used in the calculations for Si_2BN, ph-Si and h-BN is 500 eV. For these mesh cutoff value and k-grid points the total energy per atom converges to a certain value with an error which is less than 1 meV.

The structural optimization is achieved through the use of the conjugate gradient method. Optimizations are performed both for atomic positions and lattice vectors. Optimization process is assumed converged if the maximum atomic force and the maximum stress component is less than 0.005 eV $Å^{-1}$ and 0.005 GPa, respectively. Each of the Si_2BN, ph-Si and h-BN layers are simulated using supercells with layer separation of 20 Å along the z-direction.

For the calculation of the density of states (DOS) the already optimized structure is used but its eigenenergies are calculated again for a larger Monkhorst–Pack k-points grid ($70 \times 70 \times 1$). Partial density of states (p-DOS) of each atom and its valence orbitals are also obtained.

The primitive unit cells for the Si_2BN structures with AA or AB stacking each contain 8 atoms (two Si_2BN formula units) and are shown in figures 3(a) and (d), respectively. The corresponding lattice vectors are shown as red arrows. However, an optimization calculation using just 8 atom unit cells may not be sufficient to capture any possible symmetry breaking, which could possibly take place in neighboring unit cells due to the translational symmetry. In order to capture any such symmetry breaking, a rectangular 32 atom (2×2) unit cell was initially used for the optimization calculations for both structures with a $10 \times 10 \times 1$ Monkhorst–Pack k-points grid. However, no symmetry breaking was observed.

For the investigation of high temperature stability we calculate the phonon spectra at high temperatures using the *ab initio* VASP package utilizing the projector augmented wave approach to generate the plane wave basis set [51–53]. The exchange–correlation is modeled by the use of the PBE functional under the GGA [46]. To determine the equilibrium crystal structures, the Hellmann–Feynman forces on the atoms and the stress on the unit cell are minimized; the convergence criterion on energy and forces is set at 1.0×10^{-5} eV and 5.0×10^{-4} eV $Å^{-1}$, respectively. For the smearing, we have

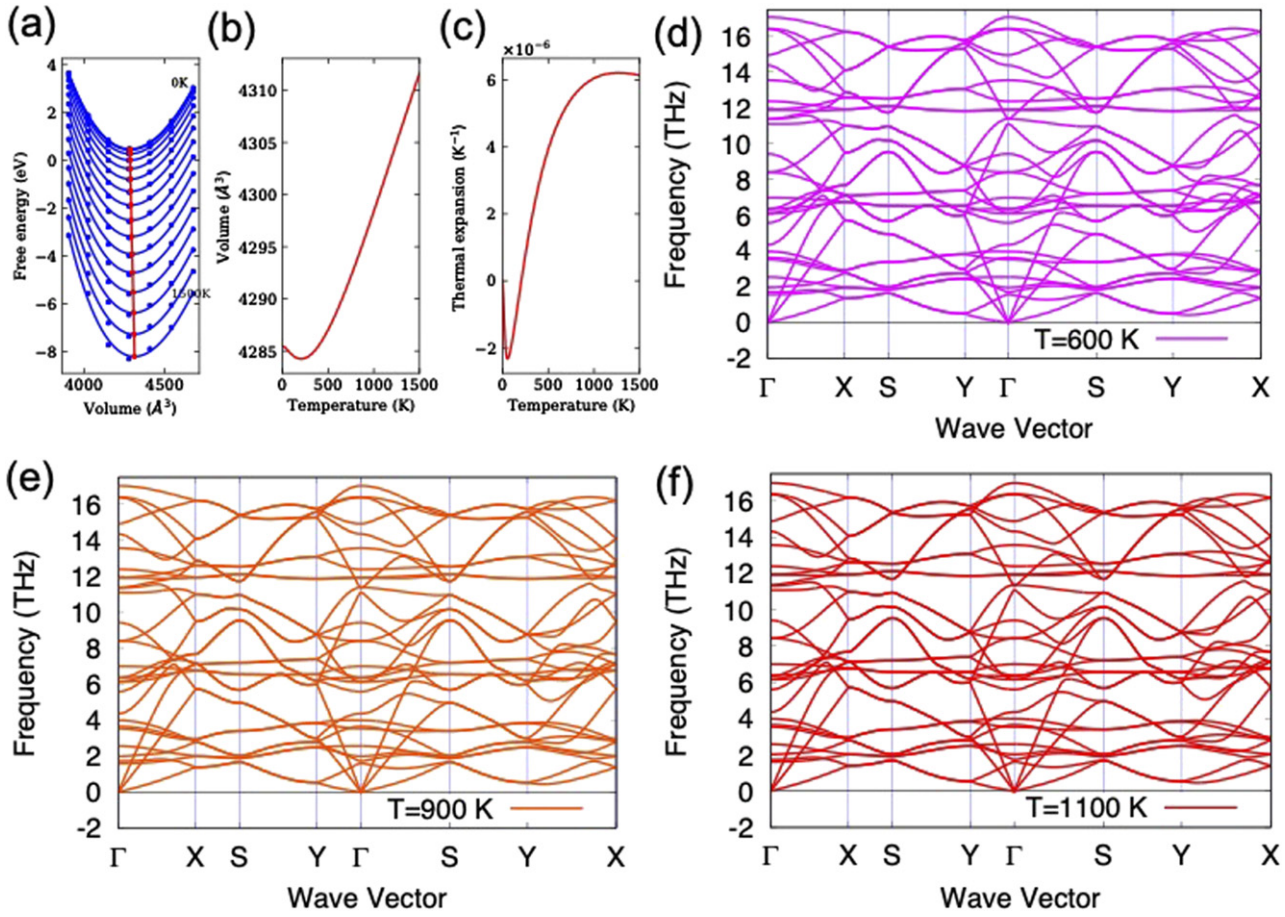

Figure 2. Phonon modes at finite temperature for the Si_2BN-AA structure. (a) The free energy curve calculated at seven different volume points. (b), (c) The volume-temperature curve and the thermal expansion curve, respectively, plotted for temperature dependence up to 1500 K. (d), (e) and (f) The finite temperature phonon dispersion plots showing the stable phonon modes at 600, 900 and 1100 K, respectively.

used the Methfessel–Paxton scheme with a smearing width of 0.2 [54]. To perform the phonon calculations, we have used supercell approach under the framework of force-constants method using the density functional perturbation theory [55]. A supercell of $2 \times 2 \times 1$ was used for the calculation of the force constants. The force-constants are further used to obtain the phonon modes by employing the PHONOPY package [56, 57].

3. Results and discussion

3.1. The structure of Si_2BN with AA and AB stacking

The energetically optimum structures of Si_2BN with AA and AB stacking are shown in figures 3(a) and (d), respectively. In accordance with what was previously found [24], Si_2BN with AA stacking is slightly more stable than Si_2BN with AB stacking. According to our calculations, the energy difference between the two structures is 0.159 eV per formula unit, or 0.040 eV per atom. The structural properties of those structures, obtained from our optimization calculations, are shown in table 1. It is worth noting that some of the structural properties using the same method for the Si_2BN structure with AB stacking have been reported elsewhere [25]. However, we present those results here again in a more systematic way for ease of comparison with those of the Si_2BN with AA stacking.

While ph-Si and h-BN which constitute a perfect honeycomb lattice, in the Si_2BN, the permutation of three different atoms gives rise to different bonds lengths (Si–Si, Si–N, Si–B and B–N) as expected. This leads to a distorted honeycomb lattice which is no longer hexagonal. According to our findings the space group symmetry of the Si_2BN structure with AA stacking is the *Pmma* one (no 51), while the Si_2BN structure with AB stacking has the *Cmmm* (no 65) symmetry, which belong to the primitive orthorhombic and base centered (BC) orthorhombic 3 dimensional lattices, respectively, or the rectangular and center rectangular 2D lattices, respectively.

The atomic positions of Si, B and N in Si_2BN structures are given in fractional coordinates through the corresponding Wyckoff positions and the lattice vector lengths (a, b and c) and angles (α, β and γ) for each structure are shown in table 1. For the Si_2BN structure with AA and AB stacking the atomic positions of Si correspond to j and q Wyckoff positions, respectively, while the atomic positions of both B and N correspond to f and h Wyckoff positions, respectively. It is worth noting that the center rectangular lattice may be expressed with

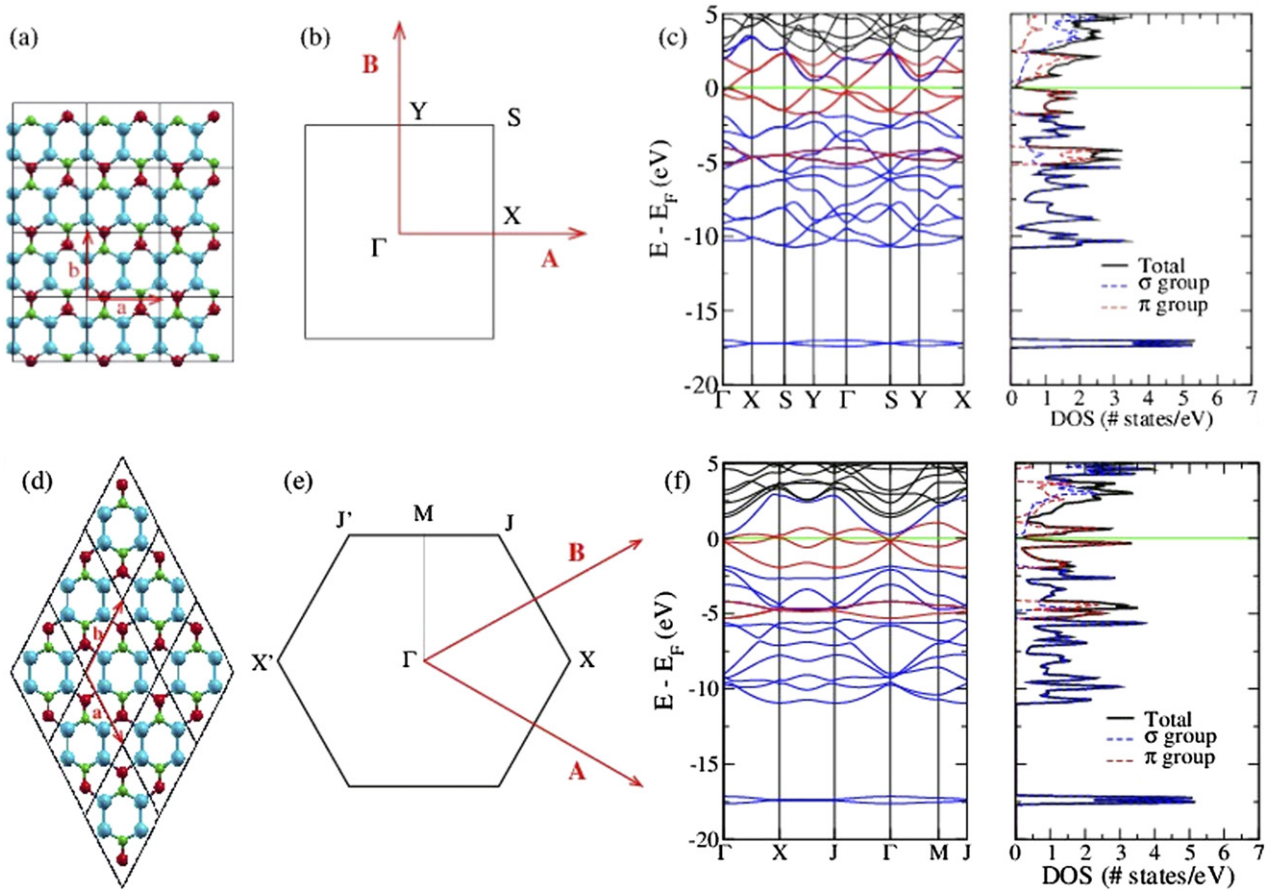

Figure 3. For Si_2BN with AA (a)–(c) and AB stacking (d)–(f). (a), (d) The primitive unit cell of the structure with the corresponding lattice vectors **a** and **b**, (b), (e) the 1st Brillouin zone with special *k*-points and the reciprocal lattice vectors **A** and **B**, (c), (f) the electronic band structure and DOS.

two different settings. One of them is orthorhombic containing 16 atoms in a unit cell, while the other is hexagonal with an 8 atom unit cell. The Wyckoff positions presented in table 1 for the Si_2BN structure with AB stacking correspond to the orthorhombic setting with the 16 atom unit cell. However, we also present the lattice vector lengths and angles for the hexagonal setting. The unit cell of the Si_2BN structure with AB stacking shown in figure 3(d) corresponds to the hexagonal setting. As can be seen from table 1, the angle γ between the lattice vectors **a** and **b** is $\gamma = 120.7619°$, which shows that the lattice of Si_2BN with AB stacking does not deviate significantly from the hexagonal lattice.

As shown in table 1, the corresponding bond lengths of the two Si_2BN structures are very close to each other. Excluding the B–N bond length which is the same for both structures, the Si–Si, Si–B and Si–N bonds of Si_2BN with AA stacking are smaller by approximately 0.1%. Comparing the Si–Si bond length of ph-Si obtained with the same parameters and method (2.281 Å) with the Si–Si bond length of Si_2BN for both stackings, we can see that the former is approximately 1% larger than the latter, indicating that the Si–Si bond of Si_2BN is stronger than that of ph-Si. The B–N bond length of h-BN (1.451 Å), however, is approximately 1% smaller than that of the Si_2BN structures indicating that B–N bonds in Si_2BN are weaker in comparison with the former. This indicates that the strengthening of the Si–Si bond responsible for stabilizing the planarity in the Si_2BN structures occurs at the expense of the B–N bonds. This is an important distinguishing feature from silicene with the weaker Si–Si bonds, which is prone to buckling.

Considering that both Si_2BN structures with either AA or AB stacking are planar and all the A–B–C angles of the structure formed by the same A, B and C atoms are the same, there are only three independent angles for Si_2BN with AA stacking and two for the Si_2BN with AB stacking. We seek and present all these angles ϕ_n through their deviations $\delta\phi_n$ from 120°, i.e. $\phi_n = 120° + \delta\phi_n$ and identify two such independent angle deviations from 120° for the structure with AB stacking (figure 1(a), top) and three for the structure with AA stacking (figure 1(b), top). Thus, if ϕ_1 = Si–B–Si, ϕ_2 = Si–N–Si, ϕ_3 = B–Si–N, ϕ_4 = N–B–Si, ϕ_5 = B–N–Si, ϕ_6 = Si–Si–N, ϕ_7 = Si–Si–B, then for both structures $\phi_3 = (\phi_1 + \phi_2)/2 = 120° + (\delta\phi_1 + \delta\phi_2)/2$, $\phi_4 = 180° - \phi_1/2 = 120° - \delta\phi_1/2$, $\phi_5 = 180° - \phi_2/2 = 120° - \delta\phi_2/2$, $\phi_6 = \phi_5 - \delta = 120° - \delta\phi_2/2 - \delta$ and $\phi_7 = \phi_4 + \delta = 120° - \delta\phi_1/2 + \delta$, where we have selected as independent angle deviations the angles $\delta\phi_1$, $\delta\phi_2$ and δ for the Si_2BN structure with AA stacking, and $\delta\phi_1$ and $\delta\phi_2$ for the Si_2BN structure with AB stacking. For the Si_2BN structure with AB stacking, $\delta = 0$ and consequently, $\phi_4 = \phi_7$ and $\phi_5 = \phi_6$. However, due

Table 2. Special points in fractional and Cartesian coordinates used for the band structure calculations of the Si_2BN structure with AA and AB stackings.

Special points	Fractional	Cartesian
AA stacking		
Γ	(0, 0, 0)	(0, 0, 0)
X	(1/2, 0, 0)	$(\pi/a, 0, 0)$
Y	(0, 1/2, 0)	$(0, \pi/b, 0)$
S	(1/2, 1/2, 0)	$(\pi/a, \pi/b, 0)$
AB stacking		
Γ	(0, 0, 0)	(0, 0, 0)
X	$\frac{1}{2\sin^2\frac{\gamma}{2}}(1, 1, 0)$	$\frac{\pi}{a\sin\gamma\sin\frac{\gamma}{2}}(1, 0, 0)$
J	$\frac{1}{1-\cos\gamma}(-\frac{1}{2}, \frac{1}{2} - \cos\gamma, 0)$	$\frac{\pi}{a\sin\frac{\gamma}{2}}(-\cot\gamma, 1, 0)$
M	$\frac{1}{4\cos\frac{\gamma}{2}}(-1, 1, 0)$	$\frac{\pi}{a\sin\gamma}(0, 1, 0)$

to the non-zero value of δ for the structure with AA stacking, the Si–Si bonds are not parallel with each other. This can be understood because in the Si_2BN with AB stacking each hexagon containing the Si–Si bonds includes both a Si–B–Si and a Si–N–Si angle. Since Si–B–Si < Si–N–Si, the Si atoms which are bonded to a B atom are closer with each other compared to the Si atoms which are bonded to the N atom. This leads to a small opposite inclination of neighboring Si–Si bonds of the same Si–Si ribbon. On the other hand, in the Si_2BN structure with AA stacking the corresponding hexagons contain either two Si–B–Si angles or two Si–N–Si angles. Therefore, the distance between the Si atoms forming the one and the other Si–B–Si (or Si–N–Si) angle of that hexagon is the same and the Si–Si bonds are all parallel with each other, although not at the same distance between each other in the ribbon. This is why $\delta = 0$ in that structure. For a similar reason all B–N bonds are parallel with each other in both structures.

It is worth noting that those angle deviations $\delta\phi_n$ from 120° are not due to the different bond lengths of the structures. The symmetry of the structure, even with those bond length differences, allows the formation of a planar geometry with all bond angles to be 120°. In other words, there is no need for stress accommodation due to the different bond lengths, which causes the bond angles to deviate from 120°. Therefore, it is evident that those deviations are due to second or higher nearest neighbor interactions. However, second nearest neighbor interactions are the same for both Si_2BN structures, which means that the different angle deviations from 120° in those two structures are due to the third or higher nearest neighbor interactions. As one can easily see, the differences between the two structures in terms of the four-atom connectivity paths are the following: the AA structure, has two B–Si–Si–N *cis* paths, two B–Si–Si–B and two N–Si–Si–N *trans* paths, while the AB structure has two B–Si–Si–B and two N–Si–Si–N *cis* paths, and two B–Si–Si–N *trans* paths. Therefore, it is evident that the basic difference between the two structure is a *cis–trans* difference, which is not only responsible for the different bond angles between the two structures, but also for their stability.

It is also worth noting that $\delta\phi_1$ and $\delta\phi_2$ are the largest angle deviations from 120° in absolute values for both structures.

3.2. High temperature stability of Si_2BN

We next investigate the thermal stability of the Si_2BN structure by studying its thermodynamic properties and phonon modes.

Specifically, we investigate the thermodynamic properties at constant volume V and study the effect of thermal vibrations i.e. phonon modes on the free energy. The Helmholtz free energy, $F(V, T)$, incorporating vibrational effects can be formulated as [57]:

$$F(V, T) = U_{\rm lat}(V) + U_{\rm vib}(V, T) - TS(V, T), \qquad (1)$$

where T is the temperature, $U_{\rm lat}(V)$ is the static contribution to the internal energy at volume V, and the term $U_{\rm vib}(V, T)$, is the vibrational contribution to the free energy coming from the vibrating phonon modes and S is the entropy due to the vibrational degrees of freedom. Within the quasi-harmonic approximation (QHA), the term $U_{\rm vib}(V, T) - TS$ can be expressed as:

$$U_{\rm vib}(V, T) - TS(V, T) = \sum_{\mathbf{q}\lambda}\left\{\frac{1}{2}\hbar\omega_{\mathbf{q}\lambda}(V) + k_{\rm B}T\ \ln \times\left[1 - \exp\left(\frac{-\hbar\omega_{\mathbf{q}\lambda}(V)}{k_{\rm B}T}\right)\right]\right\}. \qquad (2)$$

Here, the summation is over all three phonon branches λ and over all wave vectors $\mathbf{q}$ in the first Brillouin zone. The quantity $\omega_{\mathbf{q}\lambda}(V)$ is the frequency of the phonon with wave vector $\mathbf{q}$ and polarization λ, evaluated at constant volume V, $k_{\rm B}$ is the Boltzmann constant, and $\hbar$ the reduced Planck constant.

A summary of our results for the Si_2BN-AA structure are presented in figure 2 which shows the effect of finite temperature on the physical properties and establishes its thermodynamic stability beyond 1000 K.

The Helmholtz free energy F was calculated at seven different volume points for 15 different temperature values in the range [0, 1500] K with a 100 K increment. The curves of F for those different temperature values are shown as a function of volume V in figure 2(a). The red points (and by extension the red line) show the minimum F values in that temperature range as a function of volume. The volume values at which $F(T)$ is minimum are shown as a function of temperature in figure 2(b), where one can see that the volume at first decreases and then increases, indicating that the thermal expansion coefficient is initially negative for low temperatures and becomes positive as the temperature increases. This is more clearly shown in figure 2(c), where the volumetric thermal expansion coefficient is shown as a function of the temperature.

The negative thermal expansion coefficient seems to be a common feature of one-atom thick 2D structures, but not in general of all 2D structures. For instance, the thermal expansion coefficient was found to be negative both in graphene [58–61] and h-BN [60–62], but not in MoS_2 and $MoSe_2$ structures [60]. This common feature of one-atom thick 2D structures can be explained as due to the softer character of their out-of-plane vibrations (which are governed by bond angle bending), compared to their in-plane vibrations (which are

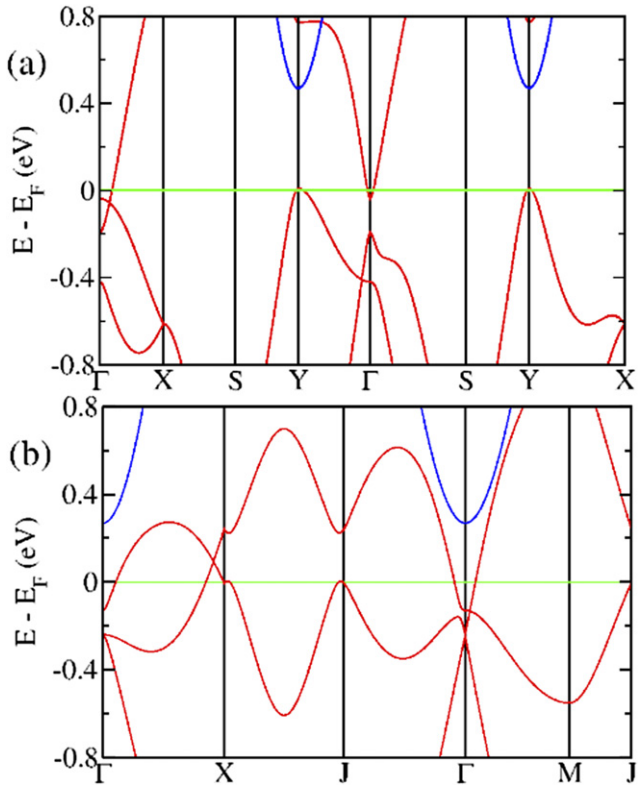

Figure 4. Band structure details around the Fermi level for Si_2BN structure with AA (a) and AB (b) stacking.

governed by bond stretching). Thus, at low temperatures, structural distortions due to bond angle bending will be more significant than those due to the bond stretching and the structure will buckle instead of vibrating in-plane, which in turn will shrink the structure causing the thermal expansion coefficient to be negative. However, as the temperature increases, distortions due to the bond stretching gain their lost ground and may become more significant than the distortions due to the bond angle bending, thus expanding the volume of the structure.

For graphene it was found experimentally that the thermal expansion coefficient remains negative in the range between 300–400 K [58], while theoretical studies reported that it can be negative even at 1000 K [59, 61]. This is not surprising since graphene is one of the strongest materials with a Young's modulus of the order of 1000 GPa [4, 25]. This means that in-plane vibrations will need a lot of energy to be activated and, therefore, in a monolayer graphene mostly the out of plane distortions occur, thus shrinking the structure (see also reference [59]). Hexagonal BN, with a smaller Young's modulus of the order of 800 GPa [25], was found to have a negative expansion coefficient up to ≈ 620 K attaining its minimum value at ≈ 250 K [62]. However, other studies report that the expansion coefficient of h-BN is negative even at 1000 K [60, 61]. Si_2BN, with an even smaller Young's modulus (of the order of 350 GPa) was found in the present study to have a negative thermal expansion coefficient up to 200 K, which exhibits its minimum value at 50 K and at room temperature (300 K) it takes the (volumetric) value 1.6×10^{-6} K^{-1}.

In figures 2(d), (e) and (f) we show the phonon dispersion relations, which were calculated in the frame of the QHA for $T = 600, 900$ and 1100 K. The absence of any imaginary (negative frequency) phonon modes up to a temperature of 1100 K confirms the thermal stability of Si_2BN-AA structure beyond 1000 K. The results for Si_2BN-AB structure are also similar, thus indicating stability for both structures even beyond 1000 K.

3.3. Electronic properties of Si_2BN with AA and AB stacking

Assuming that the Si_2BN structure with either AA or AB stacking lies along the xy plane, the unit cell vectors of the structure with AA stacking can be written as $\mathbf{a} = a(1, 0, 0)$ and $\mathbf{b} = b(0, 1, 0)$, where $a = 6.3918$ Å and $b = 5.6420$ Å (as shown in table 1), while for the structure with AB stacking in the hexagonal setting $\mathbf{a} = a(\cos(\gamma/2), -\sin(\gamma/2), 0)$ and $\mathbf{b} = a(\cos(\gamma/2), \sin(\gamma/2), 0)$, where $a = 6.4953$ Å and $\gamma = 120.761\,89^\circ$ (as also shown in table 1). The advantage of the hexagonal setting for the structure with AB stacking is that it allows direct comparisons of the band structure of the Si_2BN with AB stacking with that with AA stacking, since both unit cells contain the same number of atoms and therefore, contain the same number of band lines.

For those lattice vectors the 1st Brillouin zone as well as the special points used for the band structure calculations for each structure are shown in figure 3(b) (for the structure with AA stacking) and figure 3(e) (for the structure with AB stacking). These special points are defined in table 2. For the Si_2BN structure with AA and AB stackings the band structures are calculated along the paths $\Gamma XSY\Gamma SYX$ and $\Gamma X\mathrm{J}\Gamma\mathrm{MJ}$, respectively.

Using a $70 \times 70 \times 1$ Monkhorst–Pack grid [63] of k-points, representing the k-points of the 1st Brillouin zone of each structure, we calculate the DOS of the two Si_2BN structures. The electronic band structure and the DOS of the two Si_2BN structures are shown in figures 3(c) and (f). Figure 4 provides more details of these band structures for an energy window of ± 0.8 eV around the Fermi level.

The blue and red lines of the band structure plots, as well as the corresponding blue and red dashed lines of the DOS plots correspond to two different groups of orbitals, which we label 'σ-' and 'π-group' orbitals. The σ-group is the group of s, p_x, p_y, d_{xy}, $d_{3z^2-r^2}$ and $d_{x^2-y^2}$ atomic orbitals, while the π-group is the group of p_z, d_{yz} and d_{zx} orbitals.

The reason for separating the atomic orbitals into these two groups, is that the Hamiltonian eigenfunctions of any 2D planar structure (lying along the xy plane) can be expressed as a linear combination of the atomic orbitals of either σ- or π-group, but not as a linear combination of atomic orbitals of both groups. This can be easily shown[8], because for any 2D planar structure (in the xy plane), $\langle\Phi_\sigma|H|\Phi_\pi\rangle = 0$, where $|\Phi_\sigma\rangle$ is any σ-group orbital and $|\Phi_\pi\rangle$ any π-group orbital, which are centered on different atoms. Consequently, the Hamiltonian matrix is block diagonal with respect to those two orbital groups, resulting in the splitting of the Hamiltonian eigenfunctions into those which are linear combinations of the atomic

[8] A simple way to show this is to use the Slater–Koster expressions [64] for the $\langle\Phi_\sigma|H|\Phi_\pi\rangle$ matrix elements.

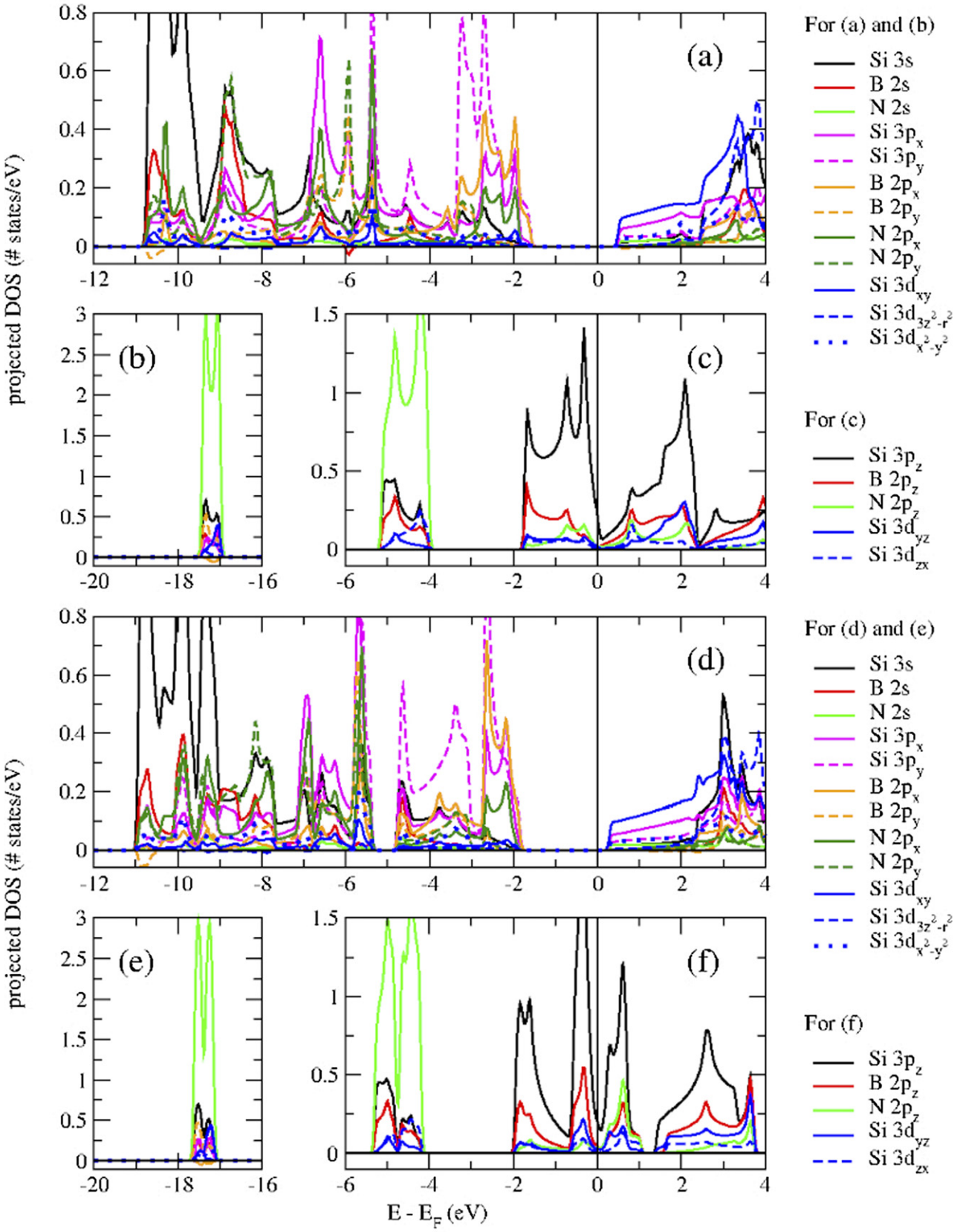

Figure 5. Projected DOS for Si_2BN orbitals with AA stacking (a)–(c) and AB stacking (d)–(f).

orbitals of σ-group and those which are the linear combinations of the atomic orbitals of π-group. Therefore, the Hamiltonian eigenstates corresponding to these two groups can be considered as independent systems, which can be studied separately. The only criteria to be satisfied is that the eigenstates of both groups below the Fermi level should be totally filled.

As can be seen in those figures, both Si_2BN structures are metallic, in accordance with previous calculations obtained using the VASP code [51] with the HSE functional (for the Si_2BN structure with AB stacking) [23], and the PBE functional (for the Si_2BN structure with AA stacking) [24]. The DOS and band structure plots contain several common features, but also notable differences. Obviously, this is not surprising due to the different atomic arrangements in the two structures as already discussed earlier.

As shown in the band structure plot of figure 4(a), the metallic character of Si_2BN with AA stacking comes from the crossing of the bands at the Fermi level near the Γ point. There are two saddle points just below the Fermi level at Γ point, at $E - E_F = -0.0374$ eV and $E - E_F = -0.1921$ eV, while there is a valence band maximum at Y point, which is slightly above the Fermi level, leaving a few empty states at Y point. As shown in the band structure plot of figure 4(b), the metallic character of Si_2BN with AB stacking comes from the bands at the Fermi level near Γ and X points. Again, there is a valence band maximum, which is slightly above the Fermi level, but now it appears near the J point. It is worth noting that none of the band maxima or minima appear exactly at these special points, but near them.

Moreover, the highest occupied state of σ-group orbitals is ≈ 1.8 eV below the Fermi level, separated by a gap with the lowest unoccupied state of the same group, which is slightly above the Fermi level. That gap is filled by π-group orbitals, as shown both in the band structure and DOS figures, and Si_2BN exhibits metallicity due entirely to the π-group of orbitals.

In order to shed more light on these results, we calculate the projected DOS (p-DOS) corresponding to the $2s$ and $2p$ orbitals of B and N, and the $3s$, $3p$ and $3d$ orbitals of Si. It is worth noting that the $3d$ orbitals of Si have a small, but non-negligible contribution to the wavefunctions of the Si_2BN. In figures 5(a)–(c) we show the p-DOS for the orbitals of the Si_2BN structure with AA stacking and in figures 5(d)–(f) the p-DOS for the orbitals of the Si_2BN structure with AB stacking. Figures 5(a), (b), (d) and (e) shows the p-DOS of the σ-group of orbitals, while figure 5(c) and (f) the p-DOS of the π-group of orbitals.

As seen in those figures, for the Si_2BN structure with the AB stacking, there are three σ-group bands separated with each other with gaps. For convenience, let us call those bands the low, the middle and the high. For the Si_2BN structure with AA stacking there are only two σ-group bands (the corresponding middle and high bands do not have a gap). In addition, for both Si_2BN structures there are two π-group of bands (the high and the low), separated by a gap of approximately 2 eV.

Counting the number of the σ- and π-group electrons, by integrating the p-DOS of the corresponding σ- and π-group orbitals up to the Fermi level, we find that there are 24 σ-group and 8 π-group electrons per unit cell (or 3 and 1 electrons, respectively, per atom on the average). Typically this is the case of conjugate sp^2 planar systems like graphene, where the s, p_x and p_y valence orbitals form strong localized σ bonds, while the p_z orbitals contributes to the delocalized p_z electron cloud through the π bonds.

Using integrations of the p-DOS for each orbital and each atom species for each band we calculate the corresponding electron count per formula unit for each case. The results we found are presented in table 3. The top and center part of that table shows the results for the σ- and the π-group orbitals, respectively, for each band described above, as well as the total count up to the Fermi level for each orbital. The total number of electrons (found by summing up the partial electron contribution of each column) is shown in the row 'total'. The expected electron count from each column is shown in the row 'expected'. The discrepancy between the values of the two rows is either due to small integration errors or the absence from those sums of the contribution from polarization orbitals, which are included in the atomic-like basis set, which is used. In the bottom part of the table, where electron counts for atom species per formula unit are presented, as well as the total electron count for both groups, contributions from all basis-set orbitals are included. In fact all the electron count values presented in table 3 are the corresponding Mulliken populations, and consequently they can only be used for a qualitative analysis of the charges due to the well known dependence of Mulliken populations on the basis set. Electron counts which are more than 0.2 electrons per formula unit are shown in bold.

Comparing the values found for each case for the Si_2BN with AA and AB stacking, we can see that they are practically the same. The maximum difference in the absolute value between the two structures is 0.054 electrons for the p_z orbitals of N. Moreover, we can see that the lower σ-group band is formed mainly by the N-$2s$ electrons with a much lower contribution from the Si-$3s$ electrons. All other orbitals have less than 0.2 electron contribution. This band clearly comes from the $2s$ states of N occupied by 2 electrons per formula unit. The middle σ-group band of Si_2BN with AB stacking corresponds to a mixture of hybridized orbitals mainly between the Si $3s$, $3p_x$, $3p_y$ and $3d_{x^2-y^2}$, the N $2p_x$ and $2p_y$ and B $2s$ and $2p_y$, while the higher σ-group band corresponds to combinations between Si $3s$, $3p_x$, $3p_y$ and B $2p_y$ orbitals. Overall, the middle and the high σ-group band do not receive a significant contribution only from the N-$2s$, Si-$3d_{xy}$ and Si-$3d_{3z^2-r^2}$ orbitals. This clearly shows that N orbitals cannot be considered as sp^2 hybridized. In contrast, it shows that N bonds have an ionic character.

On the other hand, the 2 eV gap between the high and the low π-group bands leads to the conclusion that the low π-group band does not play any role in the metallic character of the Si_2BN, as well as any other properties related with the eigenstates at the Fermi level (transport properties, excitations, reactivity, etc). Those properties, including the metallic character of the structure, are entirely derived from the high π-group band. As shown in figures 5(c) and (f), as well as in

Table 3. Electron counts per formula unit and orbital contributions to σ- and π-group bands.

σ-group Orbitals	Low AA	Low AB	Middle AB	High AB	Middle + High AA	Middle + High AB	Total AA	Total AB
Si—3s	**0.2382**	**0.2366**	**2.0254**	**0.2534**	**2.2735**	**2.2788**	2.5117	2.5154
Si—3p_x	0.0986	0.0966	**0.9201**	**0.4379**	**1.3322**	**1.3580**	1.4308	1.4546
Si—3p_y	0.0811	0.0814	**0.5882**	**0.9507**	**1.5712**	**1.5389**	1.6523	1.6203
Si—3d_{xy}	0.0944	0.1074	0.1204	0.0496	0.1775	0.1700	0.2719	02 774
Si—3$d_{3z^2-r^2}$	0.0204	0.0197	0.0024	0.0165	0.0193	0.0189	0.0397	0.0386
Si—3$d_{x^2-y^2}$	0.0487	0.0439	**0.2635**	0.0944	**0.3609**	**0.3579**	0.4096	0.4018
N—2s	**1.1456**	**1.1515**	0.0690	0.0249	0.0983	0.0939	1.2439	1.2454
N—2p_x	0.0025	0.0028	**0.8284**	0.1926	**1.0031**	**1.0210**	1.0056	1.0238
N—2p_y	0.0022	0.0027	**0.9410**	0.1345	**1.0807**	**1.0755**	1.0829	1.0782
B—2s	0.1008	0.0955	**0.5580**	0.0762	**0.6273**	**0.6342**	0.7281	0.7297
B—2p_x	−0.0129	−0.0127	0.1856	**0.5480**	**0.7420**	**0.7336**	0.7290	0.7209
B—2p_y	0.1354	0.1289	**0.4277**	0.1443	**0.5703**	**0.5720**	0.7057	0.7009
Si	0.5814	0.5856	3.9200	1.8025	5.7346	5.7225	6.3160	6.3081
N	1.1503	1.1570	1.8384	0.3520	2.1821	2.1904	3.3324	3.3474
B	0.2233	0.2117	1.1713	0.7685	1.9396	1.9398	2.1628	2.1515
Total	1.9550	1.9543	6.9297	2.9230	9.8562	9.8527	11.8112	11.8070
Expected	2	2	7	3	10	10	12	12

π-group Orbitals	Low AA	Low AB	High AA	High AB	Total AA	Total AB
Si—3p_z	**0.3207**	**0.3042**	**1.2651**	**1.2900**	1.5858	1.5942
Si—3d_{yz}	0.0486	0.0532	0.1097	0.1135	0.1582	0.1667
Si—3d_{zx}	0.1270	0.1242	0.0877	0.0796	0.2147	0.2038
N—2p_z	**1.2558**	**1.2797**	0.1356	0.0821	1.3914	1.3618
B—2p_z	**0.2025**	**0.1932**	**0.3123**	**0.3542**	0.5148	0.5474
Si	0.4963	0.4816	1.4625	1.4831	1.9588	1.9647
Total	1.9546	1.9545	1.9104	1.9194	3.8650	3.8739
Expected	2	2	2	2	4	4

	σ-group		π-group		Total	
Atoms	AA	AB	AA	AB	AA	AB
Si	6.312	6.306	1.960	1.962	8.272	8.268
N	3.379	3.396	1.420	1.395	4.799	4.791
B	2.312	2.297	0.618	0.643	2.930	2.940
Total	12.003	11.999	3.998	4.000	16.001	15.999

table 3, the low π-group band contains mainly the N-2p_z electrons, while the high π-group band contains mainly the Si-3p_z electrons. The near absence of the N-2p_z electrons from the higher π-group band ($\approx$ 0.13 and 0.08 electrons out of the 2 electrons of the band per formula unit for the structure with AA and AB stacking, respectively) shows that the N-2p_z electrons, for the most part, do not contribute to the metallic character of either SiBN structures or their properties related to the eigenstates at the Fermi level as mentioned above. These electrons are mostly localized in the 2p_z orbitals of N atoms (low π-group band), which are filled with 2 electrons per formula unit and include smaller contributions from Si-3p_z and B-2p_z electrons. Consequently, the metallic character of Si_2BN is mostly derived from the 3p_z orbitals of Si with a minor contribution from the 2p_z electrons of B.

To understand this behavior further we next compare the Si_2BN DOS with that of ph-Si and the h-BN structure.

3.4. Understanding the metallic character of Si_2BN: comparison with planar silicene and hexagonal BN

As is well known, the h-BN is an entirely planar structure [9, 21] and a wide band gap semiconductor, with its valence band mainly formed by the 2p_z electrons of N, with a minor contribution from the 2p_z electrons of B, and its conduction band mainly formed by the 2p_z energy states of B, with a minor contribution from the 2p_z states of N [9]. Silicene, on the other hand, is not planar [14, 15, 21]. However, ph-Si structure corresponds to an unstable equilibrium, and is a zero band gap semiconductor [14, 15, 21], like graphene. That ph-Si structure can be found computationally if the initial structure used for the optimization simulations remains in plane during the optimization calculation [21]. The ph-Si π-group band would be similar to that of graphene if d_{yz} and d_{zx} orbitals did not contribute to the band structure of ph-Si. Apart from this, the only difference

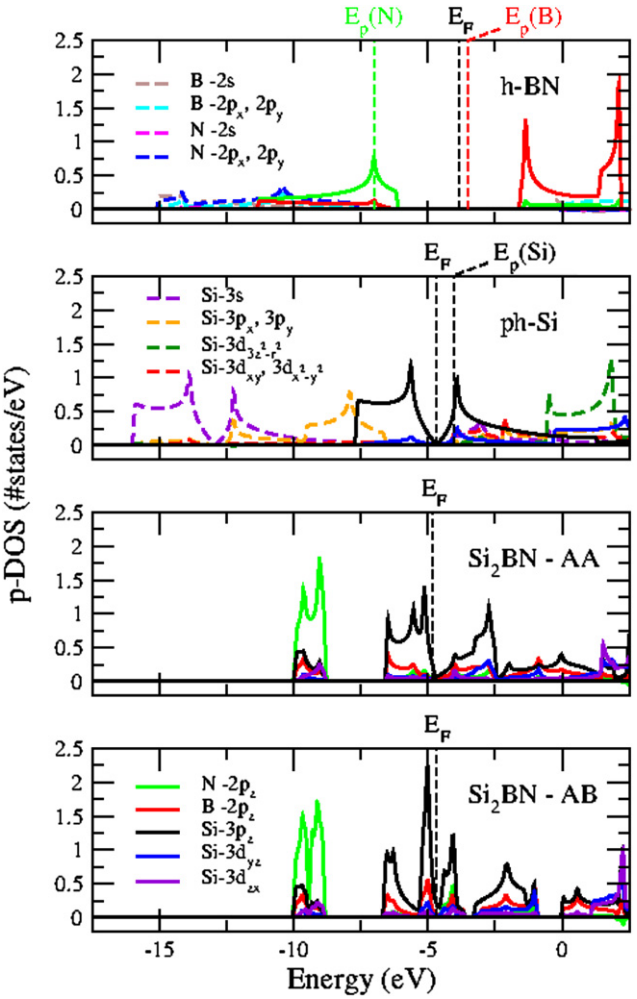

Figure 6. Projected DOS of the orbitals of h-BN (top), ph-Si (top center), Si_2BN with AA stacking (bottom center) and Si_2BN with AB stacking (bottom). The Fermi level for the h-BN is placed in the middle of the band gap. The legends of the bottom figure apply to all. The p-DOS of ph-Si for the $3p_x$ and $3p_y$ orbitals are the same. The p-DOS for group σ orbitals of h-BN and ph-Si are presented with dashed lines. The vertical dashed lines show the position of the Fermi level for each case.

between the band structure of π-group orbitals of graphene and ph-Si is the width of the bands, which would be different due to the different Si–Si and C–C bond lengths, which affect the corresponding $\langle p_z|H|p_z\rangle$ matrix elements. For instance, in terms of the Harrison's universal scheme [65] for the tight binding (TB) method, $\langle p_z|H|p_z\rangle = V_{pp\pi}(d) = \eta_{pp\pi}\hbar^2/(md^2) = -0.81 \times 7.62/d^2$ eV Å^{-2}, where d is the bond length. For ph-Si with $d = 2.28$ Å, $V_{pp\pi} = 1.19$ eV, while for graphene with $d = 1.42$ Å, $V_{pp\pi} = 3.06$ eV.

In figure 6 we present the p-DOS for the valence orbitals of the equilibrium geometries of h-BN (top panel) and ph-Si (top center panel), which were obtained using the same method as the one used for the optimizations of Si_2BN structures. In the same figure the p-DOS of the π-group orbitals of Si_2BN with AA (bottom center panel) and AB stacking (bottom panel) are also shown. For comparison between the relative positions of the electronic bands presented in those figures, the energies are not shifted with respect to the Fermi level, while the self

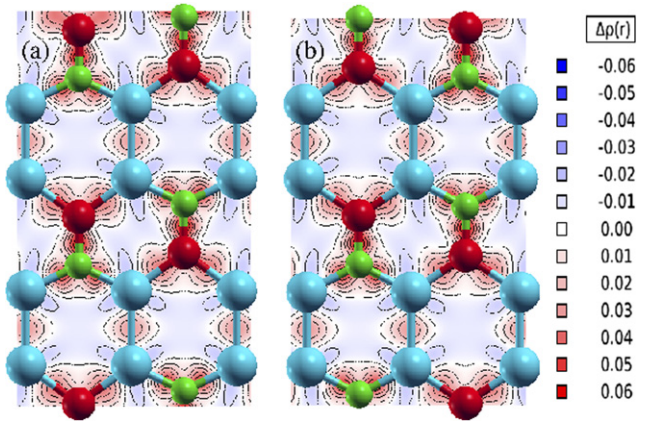

Figure 7. Electron density difference $\Delta\rho$ contour plot for Si_2BN with AA (left) and AB stacking (right).

energies (i.e. the diagonal matrix elements of the TB Hamiltonians [65]) of the $3p$ orbitals of Si and the $2p$ orbitals of B and N ($E_{Si} = -4.013\,52$, $E_B = -3.529\,02$ and $E_N = -6.984\,19$ eV, respectively), which were obtained with the same method for the isolated Si, B and N atoms are also shown.

According to what these figures show, the large energy difference between the p-orbital self energies of N and B, causes the formation of the two bands described above for the h-BN structure. As far as these two bands do not overlap and since there is only 1 valence electron per atom to occupy these bands, the lower (valence) band will be completely filled and the upper (conduction) band will be empty. This explains why the p-DOS of the p_z orbitals of h-BN looks like the one shown in figure 6 and why h-BN is a semiconductor. On the other hand, as already discussed, ph-Si behaves like graphene, i.e. it exhibits two bands separated by a zero gap, the lower one of which is totally filled with one p_z electron per atom and the higher one, which is empty.

Comparing the p-DOS of π-group orbitals of the two Si_2BN structures with those of ph-Si and h-BN, we can clearly see that qualitatively the p-DOS of the π-group orbitals of Si_2BN is a combination of the π-group orbitals of ph-Si and h-BN. The qualitative differences are: (i) the N band of h-BN has moved to lower energies due to the interactions with Si and the width of the band has decreased, (ii) the p-DOS of the $2p_z$ orbital of B has spread along the energy axis, due to the B–Si interactions and, (iii) the p-DOS of $3p_z$ orbital of Si has changed shape and introduced a few states at the Fermi level, making the Si_2BN a metal, in contrast to ph-Si which is a zero band gap semiconductor. These similarities and differences are reasonable and are due to the large energy difference between the E_p(B) and E_p(N) self energies of the p-orbitals of B and N atoms, respectively, and the fact that the self energy of Si, E_p(Si), is in between E_p(N) and E_p(B), although the energy difference between E_p(Si) and E_p(B) is small. The energy difference between E_p(B) and E_p(N) further increases the energy difference between N and B p_z band centers of h-BN, which interact with the ph-Si p_z bands, which are located in-between them. Due to those energy differences, there is not a significant modification of the bands (at least qualitatively) and this is also depicted in the character of those bands, with the

Table 4. Charge transfer (in electrons) in σ- and π-group orbitals for each atom of Si_2BN and h-BN. The negative sign indicates that the atom loses electrons, while the positive sign that it gains electrons.

	Si_2BN—(AA)			Si_2BN—(AB)			h-BN		
Atoms	σ group	π group	Total	σ group	π group	Total	σ group	π group	Total
Si	0.156	−0.020	0.136	0.153	−0.019	0.134	—	—	—
N	0.379	−0.580	−0.201	0.396	−0.605	−0.209	0.201	−0.644	−0.443
B	−0.688	0.618	−0.070	−0.703	0.643	−0.060	−0.201	0.644	0.443

lower one having mainly the N-2p_z character and the higher one the Si-3p_z character, as already discussed. If these bands had significant contributions from other orbitals, then the DOS of Si_2BN might be very different and the qualitative picture (i.e. the combination of the DOS of ph-Si and h-BN) we present, might not be correct, even qualitatively.

Thus, the lower π-group orbital band of Si_2BN, which comes from the N-2p_z band of h-BN, is totally filled with 2 electrons per formula unit, while the higher π-group orbital band of Si_2BN, which comes from the Si-3p_z band of ph-Si, is half filled with 2 more electrons per formula unit, as also is the corresponding Si-3p_z band of ph-Si. It is worth noting that the DOS differences between the structures with AA and AB stackings is due to the third nearest neighbor interactions (as already mentioned) which emphasizes the importance of these interactions in the Si_2BN case.

3.5. Bonding in Si_2BN and the role of p back donation

It is well known, that in graphene as well as in the hypothetical ph-Si, both of which have a high symmetry, hexagonal and planar 2D structures formed by the same kind of atoms, the σ-group orbitals form the well known sp^2 hybrids, which in turn form the equivalent with each other strong localized σ bonds. On the other hand, the π-group orbitals form the delocalized π bonds, which constitute the equivalently distributed electron cloud of the π-group electrons along the 2D surface of the structure. Due to the high symmetry of these structures, and in case that they do not form alternating single and double bonds (which is the case of both graphene and the hypothetical ph-Si), the electron density is equally shared among the atoms and the bonds of the structure and the bonds are purely non-polar covalent.

Similar binary structures, like the high symmetry h-BN, form the same kind of bonds, with a major difference: the bonds which are formed, are not purely non-polar, i.e. in some degree they are polar bonds, which means that neither in the σ, nor in the π bonds the electrons are equally shared among the atoms of the structure.

Moreover, in ternary (or even binary with specific atomic arrangement) similar structures (like Si_2BN), it is most likely that not only the electrons are unequally shared among the atoms, but also the bonds will not be equivalent with each other, resulting in different bond lengths. Obviously, this behavior is mainly due to the different values of the orbital self energies, or (using the more qualitative electronegativity description) due to the different electronegativities of the atoms of the structure. Following the rule according to which a bond is considered as non-polar covalent, polar covalent or ionic; if the difference between the Pauling electronegativities ΔEN of the atoms forming the bond is $\Delta EN < 0.4$, $0.4 < \Delta EN < 1.7$ and $\Delta EN > 1.7$, respectively, the Si–Si and B–Si bonds should be considered as non-polar covalent ($\Delta EN = 0$ and 0.14, respectively), and the B–N and Si–N bonds as polar covalent ($\Delta EN = 1.00$ and 1.14, respectively). [9] This unequal sharing of the electrons in the bonds of Si_2BN is clearly shown in figure 7, where isosurfaces and contours of the electron density difference $\Delta\rho$ between Si_2BN structures and the neutral Si, B and N atoms at the positions they have in the Si_2BN structures are presented.

There is, however, an interesting common feature between Si_2BN and h-BN. Assuming that before bond formations in both Si_2BN and h-BN there are 3 electrons in σ-group of orbitals in each one of B, Si and N atoms, and 0, 1 and 2 electrons in π-group orbitals, respectively, we may calculate the charge transfer in these orbital groups. Integrating the p-DOS for each orbital up to the Fermi level, we find the electrons each orbital holds. Subtracting the number of electrons these orbitals have before the bond formation, we can find the charge transfer in each group. The results found are shown in table 4.

As one can see in both Si_2BN and h-BN, B atoms loose and N atoms gain electrons in σ-group orbitals, while B atoms gain and N atoms loose electrons in π-group orbitals. This is a characteristic feature of a π back bond, which explains in several cases the planarity and the sp^2 bonding of several structures, which otherwise should form sp^3 bonds and would not be planar. The π back bonds between atoms A and B are based on the so called π *back donation*, which occurs in cases where two electrons of the σ- (or π-) group orbitals of atom A form a lone pair, while the interacting (though π back donation) σ- (or π-) group orbital of atom B is empty. When A and B are bonded through a π back bond, part of the σ- (or π-) group orbital lone pair electrons of atom A are transferred to the corresponding σ- (or π-) group empty orbital of B, while part of the π- (or σ-) group orbital electrons of atom B are transferred to the π- (or σ-) group orbitals of atom A. For instance, the recently experimentally found planar four-atom nitrogen chain in borylene-based structures [66] is attributed to the π back donation between N and B atoms, where the role of B atoms in the planarity is essential [67].

In our case, (both in h-BN and Si_2BN) the 2p_z orbital of N is filled with a lone electron pair, while the 2p_z orbital of B is empty. According to table 4, 0.20 electrons are transferred

[9] The Pauling electronegativities of B, N and Si are 2.04, 3.04 and 1.90, respectively.

from σ-group of orbitals of B to σ-group of orbitals of N, while 0.64 electrons are transferred from $2p_z$ orbital of N to $2p_z$ orbital of B, thus forming a π back bond. In turn, 0.688 and 0.703 σ-group of orbital electrons of B in Si_2BN with AA and AB stackings, respectively, are transferred to the σ-group orbitals of N and Si atoms, while 0.618 electrons are transferred back for the Si_2BN with AA stacking and 0.643 for Si_2BN with AB stacking (mainly from the $2p_z$ orbital of N to the $2p_z$ orbital of B). This is a strong indication that π back donation might be the mechanism (or one of the mechanisms) that stabilizes planarity in both h-BN and Si_2BN structures. It is worth noting that although the charge transfer in boron atoms is between 0.6 and 0.7 electrons per atom in absolute values in σ- and π-group orbitals, due to the π back donation, there is a rather small overall charge transfer in B atoms.

4. Conclusion

We have demonstrated the high temperature stability of the Si_2BN structure via the calculation of finite temperature phonon modes which show no negative contributions up to and beyond 1000 K. Our results also reveal the presence of the negative thermal expansion coefficient which appears to be a common feature of one-atom thick 2D structures. We have also presented a detailed structural analysis of the two Si_2BN stackings and provided the theoretically predicted crystallographic data for both including lattice vectors, Wyckoff positions, bond lengths and bond angles. According to our analysis the main structural differences between the two structures are the bond angle deviations from 120°, which are attributed to the third nearest neighbor interactions of *cis–trans* type. According to our findings, Si_2BN with either AA or AB stacking is metallic, behaving at the Fermi level almost as ph-Si. The metallic character of Si_2BN with AA stacking comes from the crossing of the electronic bands at the Γ point, where saddle points occur, while for Si_2BN with AB stacking it comes both form the Γ and the two *X* points (i.e. the center and two of the six corners of the almost hexagonal Brillouin zone), contrary to graphene, where its semimetallic character comes from the vertices of the Dirac cones, which appear at the six corners of its perfectly hexagonal Brillouin zone. In both structures its origin is traced to the p_z electrons of Si with a minor contribution from the p_z electrons of B, while the p_z electrons of N are well below the Fermi level, localized on the N atoms, without any significant contribution at the Fermi level and, consequently, results in the metallic character of the structure. Contrary to ph-Si which is a zero band semiconductor, the Si_2BN has a few electronic states at the Fermi level, while also possessing the advantages over silicene that it is entirely flat (i.e. without any dangling bonds) and extremely stable kinetically. From the charge transfer analysis there is a strong indication that the Si_2BN planarity is due to the π back donation between B and N atoms.

Acknowledgments

ZGF acknowledges support by the project FLAG-ERA-'GATES' (JTC-PCI2018-093137, MIS 5002772), funded by the Operational Programme 'Competitiveness, Entrepreneurship and Innovation' (NSRF 2014–2020) and co-financed by Greece and the European Union (European Regional Development Fund).

ORCID iDs

Zacharias G Fthenakis https://orcid.org/0000-0003-2661-5743
Madhu Menon https://orcid.org/0000-0002-8283-138X

References

[1] Butler S Z *et al* 2013 *ACS Nano* **7** 2898
[2] Novoselov K S, Jiang D, Schedin F, Booth T J, Khotkevich V V, Morozov S V and Geim A K 2005 *Proc. Natl Acad. Sci.* **102** 10451
[3] Geim A K and Novoselov K S 2007 *Nat. Mater.* **6** 183
[4] Fthenakis Z G and Lathiotakis N N 2015 *Phys. Chem. Chem. Phys.* **17** 16418
[5] Zhang S, Zhou J, Wang Q, Chen X, Kawazoe Y and Jena P 2015 *Proc. Natl Acad. Sci. USA* **112** 2372
[6] Enyashin A N and Ivanovskii A L 2011 *Phys. Status Solidi* B **248** 1879
[7] Crespi V H, Benedict L X, Cohen M L and Louie S G 1996 *Phys. Rev.* B **53** R13303
[8] Terrones H, Terrones M, Hernández E, Grobert N, Charlier J-C and Ajayan P M 2000 *Phys. Rev. Lett.* **84** 1716
[9] Hansson A, de Brito Mota F and Rivelino R 2012 *Phys. Rev.* B **86** 195416
[10] Lin Y and Connell J W 2012 *Nanoscale* **4** 6908
[11] Wang Q H, Kalantar-Zadeh K, Kis A, Coleman J N and Strano M S 2012 *Nat. Nanotechnol.* **7** 699
[12] Mak K F, Lee C, Hone J, Shan J and Heinz T F 2010 *Phys. Rev. Lett.* **105** 136805
[13] Liu H, Neal A T, Zhu Z, Luo Z, Xu X, Tománek D and Ye P D 2014 *ACS Nano* **8** 4033
[14] Takeda K and Shiraishi K 1994 *Phys. Rev.* B **50** 14916
[15] Cahangirov S, Topsakal M, Aktürk E, Şahin H and Ciraci S 2009 *Phys. Rev. Lett.* **102** 236804
[16] Trivedi S, Srivastava A and Kurchania R 2014 *JCTN* **11** 781
[17] Schwierz F, Pezoldt J and Granzner R 2015 *Nanoscale* **7** 8261
[18] Ding Y and Wang Y 2013 *J. Phys. Chem.* C **117** 18266
[19] Tan X, Li F and Chen Z 2014 *J. Phys. Chem.* C **118** 25825
[20] Dai J, Zhao Y, Wu X, Yang J and Zeng X C 2013 *J. Phys. Chem. Lett.* **4** 561
[21] Şahin H, Cahangirov S, Topsakal M, Bekaroglu E, Akturk E, Senger R T and Ciraci S 2009 *Phys. Rev.* B **80** 155453
[22] Nakano H, Mitsuoka T, Harada M, Horibuchi K, Nozaki H, Takahashi N, Nonaka T, Seno Y and Nakamura H 2006 *Angew. Chem., Int. Ed.* **45** 6303
[23] Andriotis A N, Richter E and Menon M 2016 *Phys. Rev.* B **93** 081413
[24] Sandoval E D, Hajinazar S and Kolmogorov A N 2016 *Phys. Rev.* B **94** 094105
[25] Fthenakis Z G and Menon M 2019 *Phys. Rev.* B **99** 205302
[26] Singh D, Gupta S K, Sonvane Y, Hussain T and Ahuja R 2018 *Phys. Chem. Chem. Phys.* **20** 21716
[27] Singh D, Gupta S K, Sonvane Y and Ahuja R 2017 *Int. J. Hydrog. Energy* **42** 22942
[28] Hu S, Yong Y, Li C, Zhao Z, Jia H and Kuang Y 2020 *Phys. Chem. Chem. Phys.* **22** 13563
[29] Shukla V, Araujo R B, Jena N K and Ahuja R 2017 *Nano Energy* **41** 251
[30] Hussain T, Singh D, Gupta S K, Karton A, Sonvane Y and Ahuja R 2019 *Appl. Surf. Sci.* **469** 775

[31] Babar V, Murat A and Schwingenschlögl U 2020 *J. Phys.: Condens. Matter* **32** 355602
[32] Javdani Z, Salehi H and Amiri P 2020 *Appl. Surf. Sci.* **527** 146941
[33] Salehi H, Javdani Z and Amiri P 2020 *Chem. Phys.* **538** 110908
[34] Yuan S-J, Zhang H and Cheng X-L 2017 *Plasmonics* **13** 947–53
[35] Rajamani A, Saravanan V, Vijayakumar S and Shankar R 2019 *ACS Omega* **4** 13808
[36] Rajamani A, Ravichandran D, Vinnarasi S and Shankar R 2020 *Mater. Lett.* **279** 128487
[37] Mahida H R, Singh D, Sonvane Y, Thakor P B, Ahuja R and Gupta S K 2019 *J. Appl. Phys.* **126** 233104
[38] Singh D, Chakraborty S and Ahuja R 2019 *ACS Appl. Energy Mater.* **2** 8441
[39] Singh D, Panda P K, Khossossi N, Mishra Y K, Ainane A and Ahuja R 2020 *Catal. Sci. Technol.* **10** 3279
[40] Chen K-X, Lyu S-S, Luo Z-Y, Fu Y-X, Heng Y and Mo D-C 2017 *Phys. Chem. Chem. Phys.* **19** 7481
[41] Freitas A, Machado L D, Tromer R M, Bezerra C G and Azevedo S 2017 *Superlattices Microstruct.* **110** 281
[42] Xie Q, Yuan J, Yu N, Wang L and Wang J 2017 *Comput. Mater. Sci.* **135** 160
[43] Drummond N D, Zólyomi V and Fal'ko V I 2012 *Phys. Rev.* B **85** 075423
[44] Zhao T, Zhang S, Wang Q, Kawazoe Y and Jena P 2014 *Phys. Chem. Chem. Phys.* **16** 22979
[45] Ouhe R *et al* 2012 *Sci. Rep.* **2** 853
[46] Perdew J P, Burke K and Ernzerhof M 1996 *Phys. Rev. Lett.* **77** 3865
[47] Soler J M, Artacho E, Gale J D, García A, Junquera J, Ordejón P and Sánchez-Portal D 2002 *J. Phys.: Condens. Matter* **14** 2745
[48] Troullier N and Martins J L 1991 *Phys. Rev.* B **43** 1993
[49] Kleinman L and Bylander D M 1982 *Phys. Rev. Lett.* **48** 1425
[50] Rivero P, Manuel García-Suárez V, Pereñiguez D, Utt K, Yang Y, Bellaiche L, Park K, Ferrer J and Barraza-Lopez S 2015 *Data Brief* **3** 21
[51] Kresse G and Furthmüller J 1996 *Phys. Rev.* B **54** 11169
[52] Kresse G and Joubert D 1999 *Phys. Rev.* B **59** 1758
[53] Blöchl P E 1994 *Phys. Rev.* B **50** 17953
[54] Methfessel M and Paxton A T 1989 *Phys. Rev.* B **40** 3616
[55] Kresse G, Marsman M and Furthmüller J *VASP The Guide* (http://cms.mpi.univie.ac.at/vasp/vasp.pdf)
[56] Togo A, Oba F and Tanaka I 2008 *Phys. Rev.* B **78** 134106
[57] Togo A and Tanaka I 2015 *Scr. Mater.* **108** 1
[58] Yoon D, Son Y-W and Cheong H 2011 *Nano Lett.* **11** 3227
[59] Bondarev V N, Adamyan V M and Zavalniuk V V 2018 *Phys. Rev.* B **97** 035426
[60] Sevik C 2014 *Phys. Rev.* B **89** 035422
[61] Mann S, Kumar R and Jindal V K 2017 *RSC Adv.* **7** 22378
[62] Cai Q *et al* 2019 *Sci. Adv.* **5**
[63] Monkhorst H J and Pack J D 1976 *Phys. Rev.* B **13** 5188
[64] Slater J C and Koster G F 1954 *Phys. Rev.* **94** 1498
[65] Harrison W A 1989 *Electronic Structure and the Properties of Solids* (New York: Dover)
[66] Légaré M-A, Rang M, Bélanger-Chabot G, Schweizer J I, Krummenacher I, Bertermann R, Arrowsmith M, Holthausen M C and Braunschweig H 2019 *Science* **363** 1329
[67] Broere D L J and Holland P L 2018 *Science* **359** 871